Particle Accelerators, 1994, Vol. 46, pp. 225–239
Reprints available directly from the publisher
Photocopying permitted by license only

QUADRUPOLE MAGNETS FOR THE FINAL FOCUS OF THE FFTB AT SLAC

H. NAKAYAMA,[1] Y. SAKAMOTO,[1] T. CHUGUN[2] and T. HARIGAI[2]

[1] *KEK, National Laboratory for High Energy Physics, 1–1 Oho, Tsukuba-shi, Ibaraki-ken, 305, Japan*

[2] *Keihin Product Operations, Toshiba Corporation, 2–4 Suehiro-cho, Tsurumi-ku, Yokohama-shi, 230, Japan*

(Received 14 December 1993; in final form 22 March 1994)

The very precise quadrupole magnets used for the final focus section of the FFTB (Final Focus Test Beam) at SLAC were fabricated and tested. Two of the three quadrupole magnets that are placed just before the focal point have strong field gradients and relatively small apertures. The ratios of the sextupole and the octupole components to the quadrupole component are limited to very small values to avoid increasing the beam spot sizes. The normal and skew octupole components, which have about several times larger limit values than those of the sextupole, can be brought within the limit by severe pole machining and assembly tolerances. However, the sextupole component limits (both normal and skew) are too small. We therefore suppressed the sextupole components to be less than 10^{-4} by independent excitations of the trim coils wound around the magnet poles.

KEY WORDS: Magnets, magnetic measurements, linear colliders

1 INTRODUCTION

As a future colliding machine[1] for continuing to explore the energy frontier in the e^+e^- interaction, the electron-positron linear collider is the subject of active research in various places throughout the world.

Linear colliders of the next generation will require a luminosity of between 10^{33} and 10^{34} $cm^{-2}sec^{-1}$, which is required to investigate very rare events. The key problems concerning the final focus system (FFS), which must be overcome in order to increase the luminosity to such an amount, are to have very small beam spot sizes and to keep the beam cross section flat at the interaction point (IP) in order to minimize the beamstrahlung radiation emitted as energetic electrons or positrons interact with the strong electromagnetic field of the opposing bunch. The FFS at the final stage of a linear collider must strongly focus beams and produce the very small flat beam size of several hundred nanometers wide and a few nanometers high at the IP. The optics of the final focus system are being actively studied. The basis of the FFS is an achromatic system for the given parameters of the incoming beam with a large geometrical demagnification factor, and with chromatic aberrations introduced into the beam at the IP controlled by local optical elements.

In order to test such a final focus scheme experimentally using the 50GeV electron beams from the SLAC linac, an international collaboration has been formed to design and construct a Final Focus Test Beam (FFTB).[2,3] The goal of the FFTB is to produce electron bunches with transverse dimensions of 1 μm wide and 60 nm high at the focal point; in addition to this, the FFTB is used to test the alignment, stability and instrumentation requirements necessary to produce small beam spots.

In this paper we describe the design, fabrication, magnetic field measurements and method of sextupole component cancellation of the three magnets (QC2, QX1 and QC1) placed just before the IP in the final transformer of the FFTB.

2 DESIGN OF MAGNETS

The FFTB beam line is composed of five optical modules; these are, from the end of the linac to the IP, the beta matching section (BM), the horizontal chromatic correction section (CCX), the beta exchange section (BX), the vertical chromatic correction section (CCY) and the final transformer (FT).[4,5,7] The three quadrupole magnets (QC2, QX1 and QC1) are placed before the IP, and are referred to as the final quadrupole doublet because the polarities of QX1 and QC1 are the same and opposite to that of QC2, which is a focusing quadrupole magnet.

These quadrupole magnets have strong field gradients and relatively small apertures, that correspond to ten sigma of the beam sizes. Especially the defocusing magnets (QC1 and QX1) produce very strong field gradients; their field strength at the pole surface are 1.2 and 1.4T, respectively, because these provide a very strong focus in order to produce very small beam spot sizes. Since the field strength of QX1 is too strong to generate a good field gradient using poles of soft iron, the poles and the return yokes are made of an alloy of iron and cobalt (Fe 49%,Co 49%,V 2%), the saturation flux density of which is about 20% higher than that of soft iron. The other two magnets are made of normal soft iron.

The field components of higher order harmonics of these magnets are limited to a very small amount. The limit values for the sextupole and octupole are determined so that the allowed increase in the spot size from the aberrations is set to 2% per aberration of one quadrupole magnet.[6,7] The upper-limit values of the sextupole and octupole field errors are listed in Table 1.

For all magnets, the allowed normal and skew sextupole fields at the pole surface relative to the quadrupole field are of the order of 10^{-4}. If we estimate the displacement errors of the poles from the allowed sextupole fields, using the first-order perturbation theory of Halbach,[8] the allowed rotational and azimuthal displacements are estimated to be very small, say 1 μm or less. It is very difficult or/and very expensive to fabricate quadrupole magnets with such small machining and alignment errors.

On the other hand, the allowed octupole relative fields are several times larger than the sextupole field. The corresponding allowed displacement errors are about 5~20 μm. Therefore, we determined that we should set the fabrication tolerances of the magnets based on the maximum octupole field errors and that we should suppress the sextupole field errors by independent excitations of four trim coils wound around each pole. This strategy lowers fabrication cost.

TABLE 1: Demands for the quadrupole magnets.

	QC1	QX1	QC2
Aperture radius R(mm)	6.5	10.0	26.0
Pole length l(mm)	1114.0	300.0	2000.0
Field gradient k(T/m)	176.9	138.0	36.7
$B^{(3)}_{\text{normal}}/B^{(2)}$ limit at R	1.2×10^{-4}	2.0×10^{-4}	1.0×10^{-4}
$B^{(3)}_{\text{skew}}/B^{(2)}$ limit at R	1.8×10^{-4}	3.2×10^{-4}	0.8×10^{-4}
$B^{(4)}_{\text{normal}}/B^{(2)}$ limit at R	6.7×10^{-4}	1.9×10^{-3}	4.7×10^{-4}
$B^{(4)}_{\text{skew}}/B^{(2)}$ limit at R	1.3×10^{-3}	1.6×10^{-3}	3.1×10^{-4}
Pole displacement (μm)	$\leq$5	$\leq$20	$\leq$13

Since the differences in the thermal expansions between poles due to the difference in the heat transfer from the coils produce unwanted higher order fields, we enlarged the cross sections of the coils in order to lower the current densities; this makes the outer sizes of magnet large.

The shape of pole and yoke of the quadrupole magnets are determined by 2-dimensional field calculations using POISSON; these are shown in Figure 1; the magnet parameters are listed in Table 2.

3 FABRICATION AND DIMENSION MEASUREMENTS

Before fabrication of QC1,QX1 and QC2, we produced a half-length model of QC1 in order to study how to machine and assemble such a precise magnet, and what structure is suitable for a precise assembly.

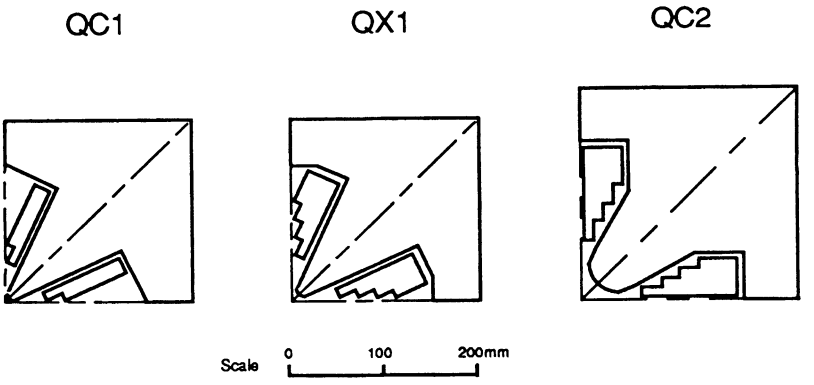

FIGURE 1: Cross sections of the quadrant of the quadrupole magnets.

TABLE 2: Parameters of the final focus quadrupole magnets.

	QC1	QX1	QC2
Yoke and pole			
Aperture radius R(mm)	6.5	10.0	26.0
Pole length l(mm)	1114.0	300.0	2000.0
Total width (mm)	400.0	400.0	460.0
Material	S10C	Fe-Co	S10C
Main coil			
No. of turns/pole	18	28	28
Max. current (A)	250	250	500
Trim coil			
No. of turns/pole	18	26	20
Max. current (A)	10	10	10

Based on the R&D, we decided that the magnet be divided into four parts by the horizontal and vertical symmetric planes. After cutting and annealing, as a final process of machining, each part of pole and yoke was ground by an NC-grinding machine. The grinding was carefully carried out by measuring the shape, straightness, flatness and dimensions of the pole as well as the split planes by a 3-dimensional coordinate measuring machine(3D-CMM), whose measurement errors were about 1μm. We could assemble the half-length model with errors of 3μm.

The same procedure was applied to the fabrication of all quadrupole magnets. The shapes and positions of the poles at both ends along the length were measured by the 3D-CMM. The deviations from the ideal curve and position are almost equal to the tolerances, or less. We show, as an example, the result of a measurement of the poles of QC1 in Figure 2.

4 FIELD MEASUREMENTS

The magnetic field of the quadrupole magnet integrated along the magnet length direction was picked up by a long one-turn coil made of thin gold-coated W wire of 50μm diameter whose rotation frequency was 2Hz. The induced voltage was amplified and filtered with a DC amplifier, and a Fourier analysis was carried out using a dynamic signal analyzer. The coordinate system that we defined is shown in Figure 3. The polarities of the poles during the measurements and the defined pole numbers are also shown.

4.1 Excitation measurements

The excitation curves for three quadrupole magnets were obtained by measurements of the voltage signal from the quadrupole field component. Since we did not measure the field distributions along the magnet length, the coil calibrations were carried out assuming that

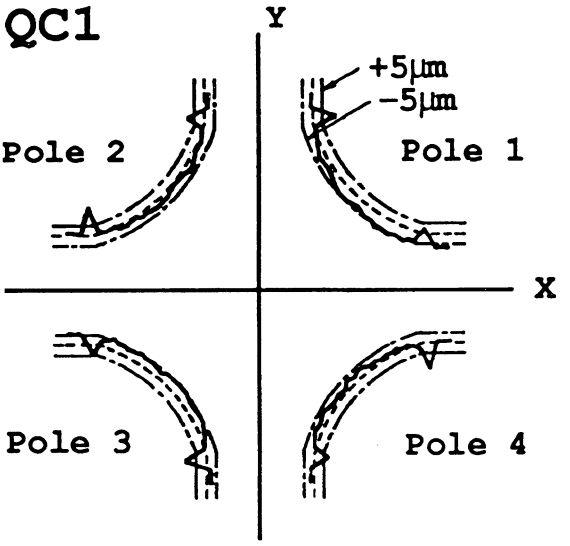

FIGURE 2: Shapes and displacements of the poles of QC1 measured by the 3D-CMM. The dashed lines indicate the ideal shape and position, and the dot-and-dashed lines indicate the allowable errors.

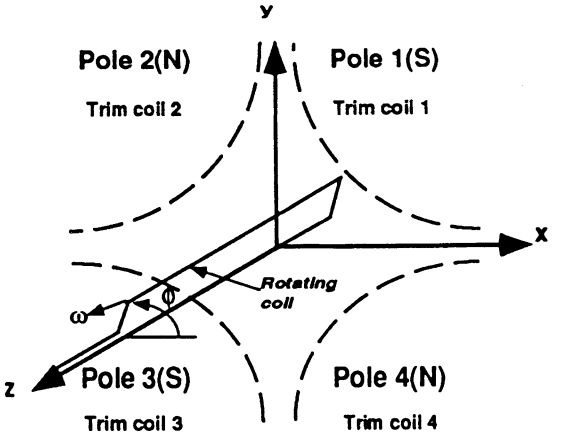

FIGURE 3: Definition of the coordinate system, pole number and polarity.

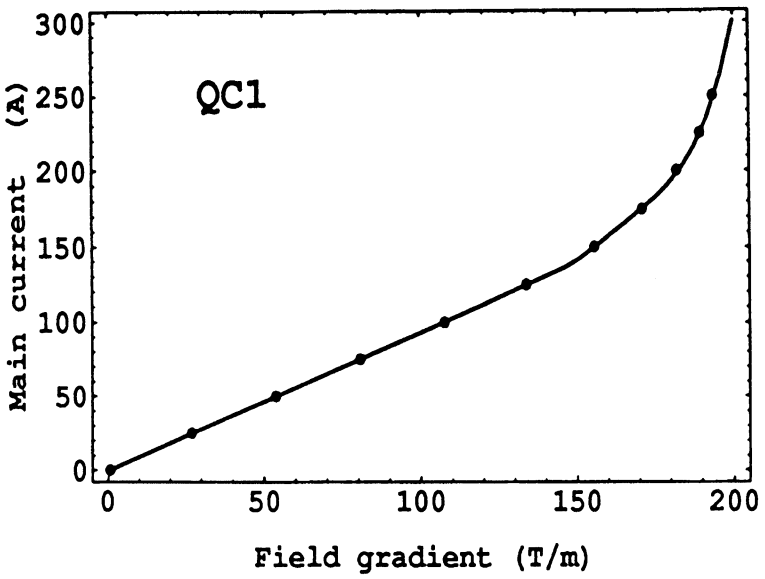

FIGURE 4: Excitation curve of QC1. The solid line is a least-squares fitted curve.

the increasing ratio of the field gradient in the non-saturated region is equal to that of the 2-dimensional field calculation, and that the integrated value is proportional to the field gradient.

In Figure 4, we show the excitation curve of QC1. For convenience of the current setting, we determined the curve of the excitation current (I) as a function of the field gradient (k); we assumed the curve can be expressed as

$$I = \begin{cases} c_1 + c_2 k & (k \leq c_3) \\ c_4 + c_5 k + c_6 k^2 + c_7 k^3 + c_8 k^4 & (k > c_3) \end{cases},$$

where c_i are constants and with the condition that the two functions and their derivatives have the same values at $k = c_3$. This condition reduces the number of constants to six. The six constants were determined by a least-squares fit; this curve is also indicated by the solid line in the figure.

4.2 Harmonic components measurements

We measured integrated harmonics of the magnetic field of the quadrupole magnets with a long rotating coil at several excitation currents. Although the trigger pulses for the start of sampling were generated when the coil wire crossed the xz-plane($x > 0$), the actual sampling began a little after the trigger pulse; the time delay depends on the setting of the

frequency range of the dynamic signal analyzer. Since it is very difficult to coincide the sampling start time with the wire crossing time, due to the reason mentioned above, we could not measure the normal and skew quadrupole components separately. We therefore assumed that only the normal quadrupole component exists, and we normalized the higher order harmonic components with the normal quadrupole component.

We made the fluctuations of the rotating speed of the coil as small as possible by using precisely aligned air bearings, which support the coil, and by using a servo motor, the rotation speed of which is controlled by an encoder output signal. However, we observed a small variation on the order of 10^{-4} in the rotation speed, which can be written as

$$\omega = \omega_0 \left(1 + \sum_{m=1} a_m \cos\left(m(\phi + \gamma)\right) \right),$$

where ϕ is the azimuthal angle. Since the radial component of the magnetic field is expressed as

$$B_r = \sum_{n=1} b^{(n)} \cos\left(n\phi + \delta_n\right),$$

the induced voltage becomes

$$\begin{aligned} V \propto\ & r_c \omega_0 \sum_{n=1} b^{(n)} \cos\left(n\phi + \delta_n\right) \\ & + r_c \omega_0 \sum_{m,n=1} \frac{a_m b^{(n)}}{2} \{\cos\left((n+m)\phi + m\gamma + \delta_n\right) \\ & + \cos\left((n-m)\phi - m\gamma + \delta_n\right)\}, \end{aligned}$$

where r_c is the radius of the rotating coil. Thus, the harmonic components of this perturbation couple with the large quadrupole signal and generate false components on the order of 10^{-4}. In the measurements, since the phase and the amplitude of false harmonics were constant, the false component moved on a circle around the unperturbed value in a phase plane, the abscissa and the ordinate of which denote the normal and skew components of the harmonics, when we changed the angle between the coil plane and the phase of the rotation of the servo motor, which corresponds to changing γ. We, therefore, carried out measurements by changing the angle, and deduced the unperturbed values by least-squares fitting of a circle.

Another source of false harmonics is a displacement of the coil rotation axis with respect to the magnetic center.[9] When the rotation axis is displaced parallel to the field axis, the false signal of an N-th order is generated from an $2n$-pole field component. The amplitude of the false signal is

$$|B^N_{\text{false}}| = \binom{n-1}{m} \rho^m |B^{(n)}|_{\rho=\rho_c}, \qquad N = n - m, \qquad 1 \le m \le n-1,$$

where ρ_c and ρ are the coil radius and the displacement normalized by the aperture radius. If we make ρ sufficiently small, the remaining false component is mainly dipole component, which is generated by a strong quadrupole component in a quadrupole magnet. Since in our measurements we set ρ to be of the order of 10^{-3}, the perturbations to the sextupole and the higher order harmonics are considered to be negligibly small.

By the method mentioned above, we deduced the normalized normal and skew coefficients of the n-th harmonic component at the aperture radius: $a_n/|a_2|$ and $b_n/|a_2|$.

The magnetic field in the aperture is expressed as

$$B_r\left(\frac{r}{R}\right) = -\sum_{n\geq 1} |B^{(2)}| \left(\frac{r}{R}\right)^{n-1} \left\{ \frac{a_n}{|a_2|} \sin(n\phi) + \frac{b_n}{|a_2|} \cos(n\phi) \right\},$$

$$B_\phi\left(\frac{r}{R}\right) = -\sum_{n\geq 1} |B^{(2)}| \left(\frac{r}{R}\right)^{n-1} \left\{ \frac{a_n}{|a_2|} \cos(n\phi) - \frac{b_n}{|a_2|} \sin(n\phi) \right\},$$

where R is the aperture radius and $|B^{(2)}|$ is the absolute value of the quadrupole field at the aperture radius. From the assumption and the polarity shown in Figure 3, $b_2/|a_2| = 0$ and $a_2/|a_2| = -1$. For all of the quadrupole magnets we observed shifts of the dipole, sextupole and dodecapole components as the pole saturates; this may have been due to a slight difference in the saturation properties of the poles (about $1\sim 2\%$ difference). However, we could not observe clear shifts of the octupole and decapole components.

The measured coefficients at the maximum excitation current of QC1,QX1 and QC2 are listed in Table 3; as an example, the phase plane plots of coefficients of $n = 3$ and $n = 4$ of QC2 are shown in Figure 5. The normal and skew octupole components of QC1 and QC2 are within the limit values given by optics calculations, as we expected from the measured deviation of the pole position. However, for QX1, the octupole components are slightly larger than those expected based on the position measurements. This may result from the fringe field region, since the ratio of the length to the aperture radius of QX1 is smaller than those of the other magnets.

5 SEXTUPOLE COMPONENTS SUPPRESSION

As mentioned previously, we could not keep the sextupole components within the tolerances which are given by optical calculations, because the corresponding machining and assembly errors are too small. Therefore, in order not to increase the beam spot sizes at the focal point, we must suppress both the normal and skew sextupole components by some method. This can be done with independent excitations of four trim coils wound around the poles.[10]

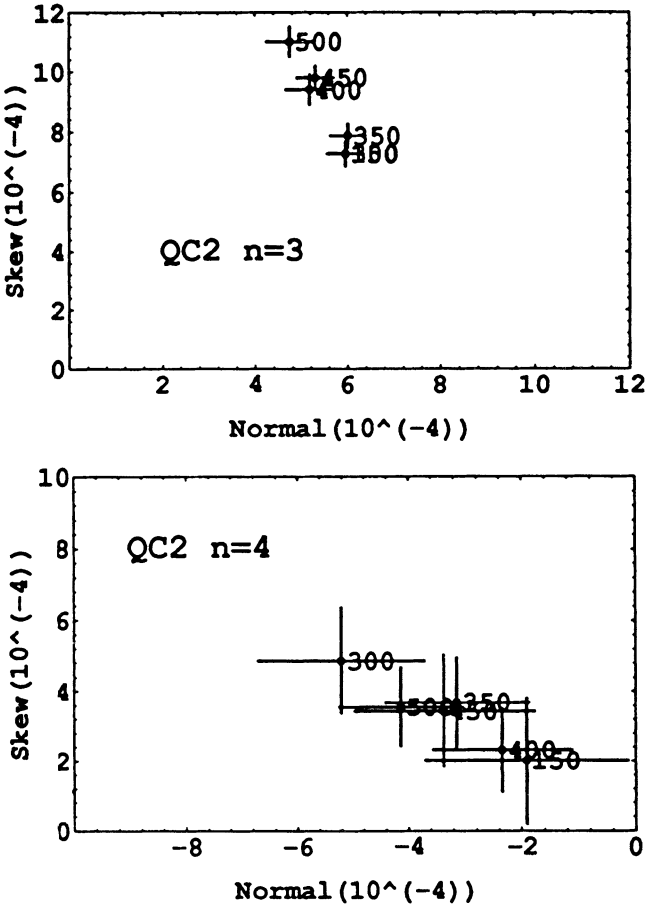

FIGURE 5: Phase plane plots of the measured sextupole and octupole coefficients of QC2. The numerals labeled give the values of the main excitation currents.

According to the perturbation theory of Halbach,[8] excitation of the k-th pole of a quadrupole magnet(see Figure 6) generates the n-th harmonic field. The generated field at the aperture radius normalized by the quadrupole field is expressed as

$$\Delta B_n = \left(\frac{n}{N}\right) j_n \exp\left\{\frac{-in\pi(2k-1)}{4}\right\} (i\varepsilon), \qquad k = 1, 2, 3 \text{ and } 4,$$

TABLE 3: Measured normalized coefficients of harmonics at the maximum current.

	Harmonics (n)	$a_n/\|a_2\|(10^{-3})$	$b_n/\|a_2\|(10^{-3})$
	3	0.82 ± 0.05	1.23 ± 0.05
QC1(250A)	4	-0.20 ± 0.18	0.79 ± 0.15
	5	-0.48 ± 0.18	-0.23 ± 0.20
	6	12.30 ± 0.70	-1.50 ± 1.12
	3	0.92 ± 0.25	0.40 ± 0.26
QX1(250A)	4	0.64 ± 0.66	2.63 ± 0.63
	5	-4.35 ± 1.03	2.31 ± 1.01
	6	12.39 ± 3.51	-0.35 ± 5.42
	3	0.48 ± 0.05	1.10 ± 0.05
QC2(500A)	4	-0.41 ± 0.11	0.36 ± 0.11
	5	0.39 ± 0.07	-0.44 ± 0.07
	6	3.76 ± 0.20	0.15 ± 0.20

where ε is a real number representing the additional excitation of the k-th pole normalized by the main excitation; $N = 2$ in this case. Here, the positive ε is the excitation which increases the magnetic scalar potential of the pole. The coefficients $(\frac{n}{N})j_n = (\frac{n}{N})\frac{\Delta C_n(x)}{i\varepsilon}$ were calculated and are listed in the table in Halbach's paper.[8] The normal and the skew components of the field correspond to $\Re(\Delta B_n)$ and $\Im(\Delta B_n)$, respectively.

In the normal-skew phase plane, a trim coil excitation produces a vector. For a sextupole, the generated components produce a vector which is expressed as $(\frac{3}{2})j_n\varepsilon \exp\left\{\frac{i(2k-3)\pi}{4}\right\}$. In Figure 6, we show this situation together with the case of other harmonics. We can generate any vector with excitations of pole 1(or/and pole 3) and pole 2(or/and pole 4). Therefore, we can suppress the inherent sextupole components of the quadrupole magnet by excitations of the trim coils. By this suppression, other harmonics, mainly the dipole and quadrupole components, are also generated. As for the quadrupole component, if we set $I_1 = -I_3$ and $I_2 = -I_4$, the additional quadrupole strength generated by each pole cancels each other(see Figure 6). The additional dipole components move the magnetic center. However, if the error sextupole and the error dipole components come from the same source (say, a slight difference in the saturation character of the pole material), the additional dipole components will also be suppressed by this method.

We measured the dependence of the amplitude of the generated harmonics on the trim-coil excitations in order to experimentally determine the coefficient $\{\frac{n}{N}j_n\}_{\text{exp.}}$.

We assume that a vector $\overrightarrow{A_n}(a, b)$ in the phase plane expresses an inherent n-th harmonic component of a quadrupole magnet. Also, the excitation of one trim coil generates another vector of the n-th harmonic component, whose amplitude is proportional to the current of the trim coil (I_t); as mentioned above, this vector is expressed as $\overrightarrow{B}_n\left(\frac{cI_t}{\sqrt{2}}, \frac{cI_t}{\sqrt{2}}\right)$, where

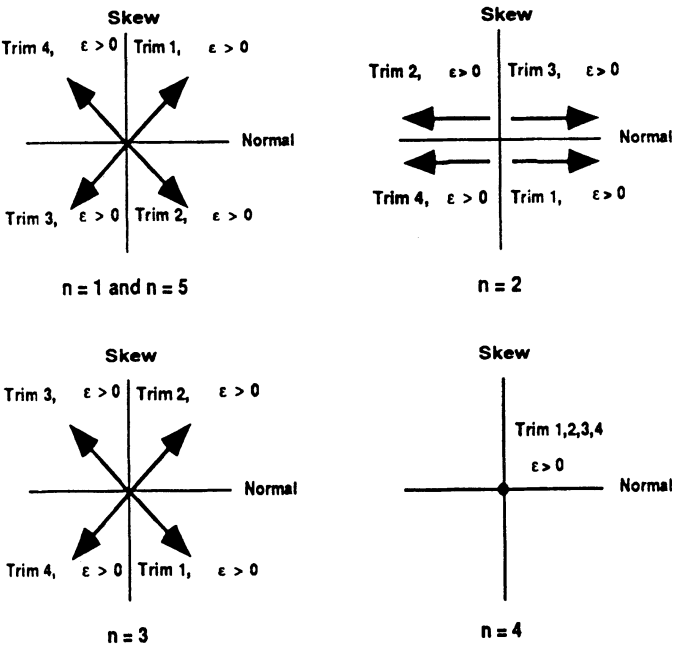

FIGURE 6: Generated vectors by excitations of the trim coils. The trim coil current that increases the magnetic scalar potential of a pole means $\varepsilon>0$. Since the coefficient $(n/N)j_n$ is negative for $n=5$, the generated vectors by trim coils 1,2,3 and 4 have the same directions as in the $n=1$ case.

c is a constant to be determined. The square of the amplitude of the summed vector $\vec{C}_n = \vec{A}_n + \vec{B}_n$ is

$$|\vec{C}_n|^2 = \left(a + \frac{cI_t}{\sqrt{2}}\right)^2 + \left(b + \frac{cI_t}{\sqrt{2}}\right)^2$$

$$= (cI_t)^2 + (a+b)(cI_t)\sqrt{2} + a^2 + b^2,$$

which is a quadratic function of I_t. In Figure 7, we show the dependence of the squares of the amplitude of the harmonics of $n = 1$ and $n = 3$ of QX1 on the trim coil current; the solid lines are least-squared curves of quadratic functions of I_t. For $n = 4$, 5 and 6, we could not find any clear dependence, as expected by Halbach's theory.

From the value of c for $n = 3$ and the measured sextupole components, we obtained the trim coil current of each pole in order to suppress the sextupole components, these are shown in Figure 8 as the functions of the main coil current. The curves are fitted curves in the same procedures as stated previously, assuming that the curve is expressed by a linear and a quadratic function.

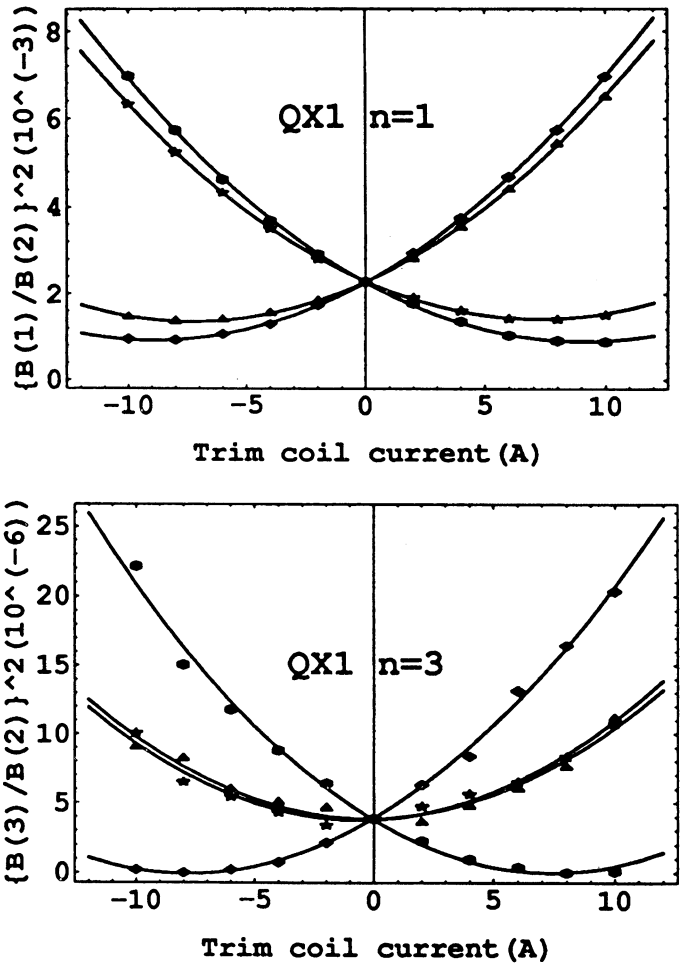

FIGURE 7: Trim-coil current dependence of the squared relative amplitudes of n=1 and n=3 of QX1. The symbols (triangle, diamond, star and hexagon) indicate the data of trim coil 1, 2, 3 and 4, respectively. The solid lines are least-squared fitted quadratic curves.

Since the additional excitation (ε) is expressed as $\varepsilon = \frac{N_t I_t}{N_m I_m}$, where N_t and N_m are the number of turns of the trim coil and the main coil and I_m is an excitation current of the main coil, c is expressed as

$$c = \frac{N_t}{N_m I_m} \left\{ \frac{n}{N} j_n \right\}_{\text{exp.}}$$

As the function of the main excitation current for $n = 1$ and $n = 3$ of QX1 and QC2, the ratios of $\left\{\frac{n}{N} j_n\right\}_{\text{exp.}}$ to $\left\{\frac{n}{N} j_n\right\}_{\text{theo.}}$, which is given by Halbach,[8] are shown in Figure 9.

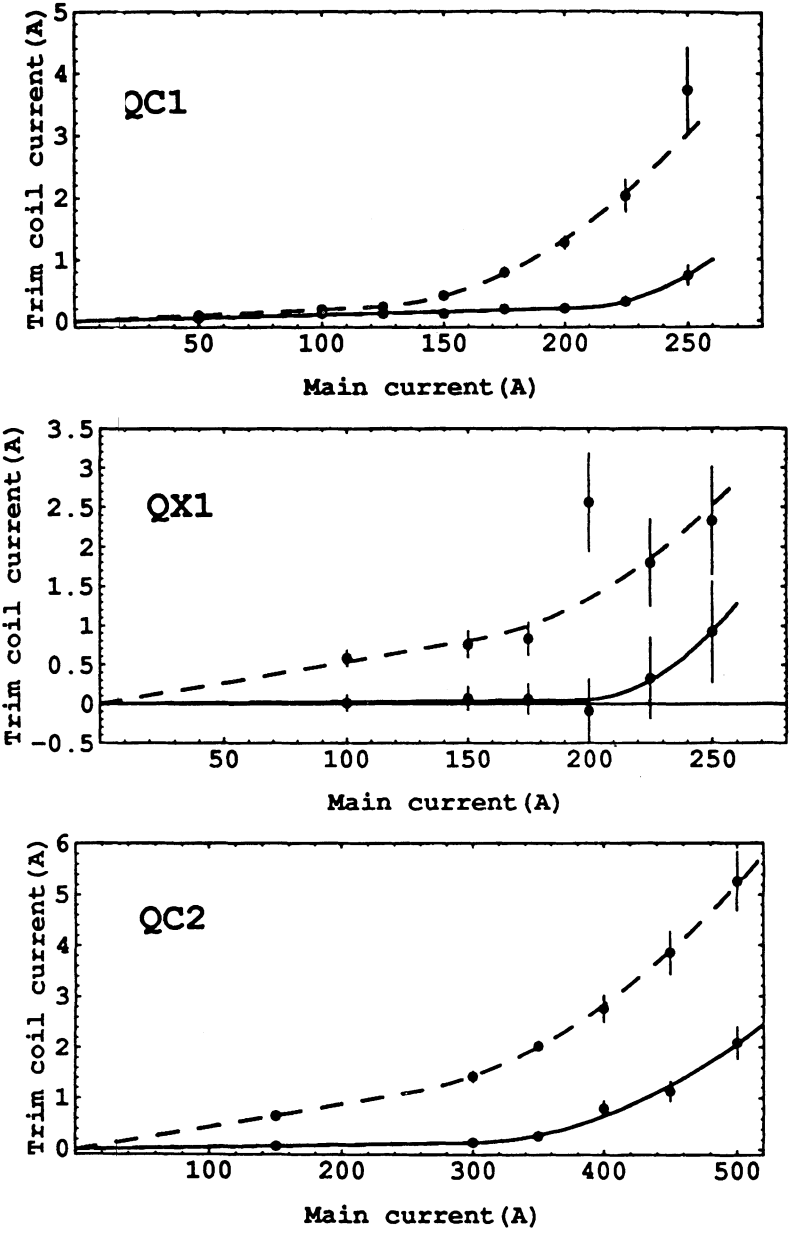

FIGURE 8: Trim-coil current for suppression of the inherent sextupole components. The solid lines are for trim $1(I_1)$ and trim $3(-I_3)$. The dashed lines are for trim $4(I_4)$ and trim $2(-I_2)$. In order not to change the quadrupole strength, the relations $I_1 = -I_3$ and $I_4 = -I_2$ must hold.

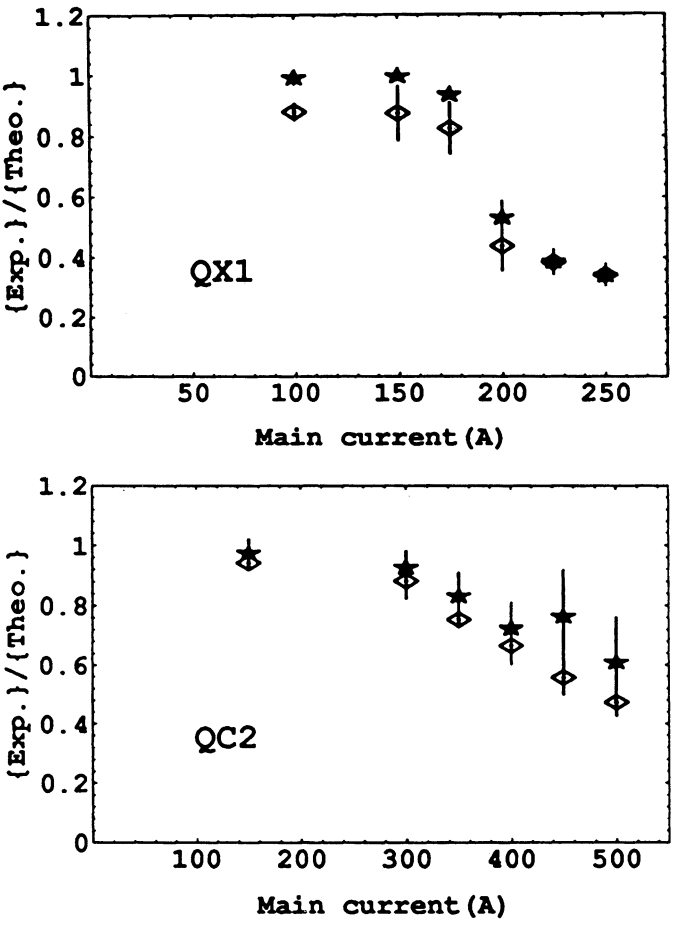

FIGURE 9: Main current dependence of the ratios of $\left\{\frac{n}{N} j_n\right\}_{\text{exp.}}$ to $\left\{\frac{n}{N} j_n\right\}_{\text{theo.}}$ of QX1 and QC2. The stars and diamonds denote the dipole and sextupole case, respectively.

The ratios for both cases are $0.9 \sim 1.0$ in the non-saturated region, but decrease as the iron core becomes saturated.

9 CONCLUSION

We fabricated very precise quadrupole magnets (QC1,QX1 and QC2) for the final focus lenses in the FFTB line and measured the integrated harmonic components of the magnetic field. The magnets were machined and assembled with errors of about 5,10 and 15 μm for QC1,QX1 and QC2, which are almost the same or slightly smaller than the machining and assembly tolerances given by the limit values of the octupole components. However,

the tolerances are not sufficient to make sextupole components smaller than the values given by the optics calculations. The sextupole components were therefore suppressed by independent excitations of the trim coils wound around the poles. This method can be applied to cases in which machining and assemble tolerances are too small to make the sextupole components small.

We found that the first-order perturbation theory by Halbach[8] is very useful to estimate the machining and assembly tolerances and to estimate the trim coil current for cancellation of the dipole and/or sextupole components.

ACKNOWLEDGEMENTS

The authors are grateful to the members of the FFTB collaboration group, especially to Prof. D. Burke and to Dr. D. Waltz at SLAC for their useful suggestions and discussions. We also want to express our thanks to Prof. K. Oide and Dr. N. Yamamoto for their suggestions concerning the optics and to Prof. S. Koizumi for his discussion concerning the machining method of magnets. The authors also want to express their thanks to Prof. H. Sugawara, Prof. Y. Kimura and Prof. K. Takata for their encouragement and support.

REFERENCES

1. R.D. Ruth, *Next Linear Collider*, SLAC-PUB-5406 (1991).
2. FFTB Collaboration group, *FFTB Project Design Report*, SLAC-376 (1991).
3. D. Burke, *The FFTB Project* (SLAC-PUB-5517, IEEE Particle Accelerator Conf., (San Francisco, 1991).
4. K. Oide, *Design of Optics for FFTB at SLAC*, SLAC-PUB-4953 (1989).
5. J. Irwin *et al.*, *The Optics of the FFTB* (SLAC-PUB-5539, IEEE Particle Accelerator Conf., (San Francisco, 1991).
6. K. Oide, *Private communication.*
7. G.J. Roy, *Analysis of the Optics of the Final Focus Beam Using Lie Algebra Based Techniques*, Ph.D. thesis, SLAC-Report-397 (1992).
8. K. Halbach, "First Order Perturbation Effects in Iron-Dominated Two-Dimensional Symmetrical Multipoles", *Nucl. Instr. Methods*, **74** (1969) 147–164.
9. R.D. Fyvie and D.E. Lobb, "An Analysis of Short Rotating Coil Measurements in the Fringe Field of a Quadrupole Magnet, *Nucl. Instr. Methods*, **114** (1974) 609–614.
10. H. Nakayama and Y. Sakamoto, *Field Measurement of the Test Quad for FFTB*, Proceedings LC91 (Protovino, 1991) 170–194.